J Electroceram (2007) 19:273–280
DOI 10.1007/s10832-007-9032-7

Noncentrosymmetric phase of submicron $NaNbO_3$ crystallites

Y. Shiratori · A. Magrez · K. Kasezawa · M. Kato · S. Röhrig · F. Peter · C. Pithan · R. Waser

Received: 4 March 2006 / Accepted: 5 January 2007 / Published online: 28 February 2007

Abstract The temperature and pressure characteristics of a noncentrosymmetric crystal modification of $NaNbO_3$ were studied by Raman spectroscopy. A transition towards the bulk-like structure of $NaNbO_3$ occurs in the temperature range from 280 to 360 °C. High-pressure Raman spectroscopy revealed successive pressure-induced phase transitions at around 2, 6.5 and 10 GPa. Raman scattering profiles recorded above 7 GPa correspond to those reported for the bulk. The temperature-induced spectral changes were completely reversible between −150 and 450 °C. Those induced by pressure were almost reversible from ambient pressure up to 15.9 GPa. Piezoresponse force microscopy demonstrated the occurrence of piezoelectric activity for submicron $NaNbO_3$ crystals with particle size ranging from 200 to 400 nm. The noncentrosymmetric crystallographic structure plays a critical role for the enhancement of piezoelectricity.

Keywords Niobates · Phase transition · Raman spectroscopy · Piezoelectricity · Size effect

Y. Shiratori · S. Röhrig · F. Peter · C. Pithan · R. Waser
Institut für Elektronische Materialien,
Institut für Festkörperforschung (IFF),
Forschungszentrum Jülich GmbH,
52425 Jülich, Germany

A. Magrez
Laboratoire des Nanostructures et des Nouveaux Matériaux Electroniques (LNNME), Ecole Polytechnique Fédérale de Lausanne (EPFL), CH-1015 Lausanne-EPFL, Switzerland

K. Kasezawa · M. Kato
Department of Applied Chemistry,
Faculty of Science and Engineering, Ritsumeikan University,
1-1-1 Nojihigashi, Kusatsu, Shiga 525-8577, Japan

Present address:
Y. Shiratori (✉)
Department of Chemical System Engineering,
School of Engineering, The University of Tokyo,
7-3-1 Hongo, Bunkyo-ku, Tokyo 113-8656, Japan
e-mail: y-shiratori@chemsys.t.u-tokyo.ac.jp

1 Introduction

The effort for substituting lead containing piezoelectric compounds such as lead zirconium titanates (PZTs) has been driven forward energetically in recent years [1–6]. High piezoelectric performance of $\{(K_{0.50},Na_{0.50})_{1-x}Li_x\}(Nb_{1-y}Ta_y)O_3$ ceramics were reported at the morphotropic phase boundary between an orthorhombic and tetragonal modification of this mixed crystal system [2]. Moreover, a ceramic of the composition $(K_{0.44}Na_{0.52}Li_{0.04})(Nb_{0.86}Ta_{0.10}Sb_{0.04})O_3$ prepared through the molten-salt synthesis method followed by a topochemical reaction and reactive-templated grain growth in combination with tape casting was textured along the <001> direction and showed excellent piezoelectric charge sensor constant (d_{33}) and piezoelectric coupling constant (k_p), both comparable to those for PZTs. However, generally, alkali niobate based ceramics are known to have a rather poor sinterability. In addition the chemical composition of the reported mixed niobate–tantalate based ceramic is quite complex in comparison to simple ternary oxides. Therefore, processing and characterization of lead-free nanocrystalline piezoelectric materials, with simple composition, having improved sinter activity, is one part of the emerging and rapidly growing field of nanotechnology. In this context we developed a method based on microemulsion mediated synthesis in order to prepare nano-crystalline powders for the preparation of electroceramic materials [7, 8]. This

method is a wet chemical route in which particle nucleation and growth are confined in aqueous micelles (hydrolysis of mixed metallic alkoxide precursors).

$KNbO_3$, one of the end members in the potassium sodium niobate system reveals the same phase transition behaviour [9], which is also typical for the perovskite ferroelectric model phase $BaTiO_3$. $NaNbO_3$ on the other hand, shows a much more complex transition characteristic through the displacement of Nb ions and tilting of NbO_6-octahedra [10, 11]. At room temperature, this material is antiferroelectric [9] but certain other oxides dissolved in $NaNbO_3$ promote a transition from the antiferroelectric to the ferroelectric state [9, 12, 13]. Recently we found a noncentrosymmetric crystal structure of $NaNbO_3$ for crystallites with reduced dimensions (200–400 nm) [14]. X-ray powder diffraction (XRPD) patterns recorded at room temperature for the coarse powders were refined with an orthorhombic *Pbcm* (D_{2h}^{11}, no. 57) structure, which corresponds to the bulk structure [15]. Below an average particle size of 400 nm, the crystal structure holds the $Pmc2_1$ (C_{2v}^{2}, no. 26) space group, which is noncentrosymmetric. Finally, fine powders with an average particle diameter of below 70 nm show a structure described by the centrosymmetric *Pmma* (D_{2h}^{5}, no. 51) space group.

The thermodynamic stability of the noncentrosymmetric phase obtained for the submicron $NaNbO_3$ crystallites is unknown up to now. For this reason the present study investigates the phase transition behaviour of this structure in dependence of temperature and pressure. These aspects are technically interesting since ceramic grains in the submicron range are expected to show enhanced piezoelectric activity. In order to monitor the structural transitions induced by these intensive variables, we apply temperature- and pressure-tuning Raman spectroscopy to submicron $NaNbO_3$ crystallites. Finally piezoresponse force microscopy (PFM) is performed, yielding in preliminary results which indicate indeed an enhancement of piezoelectric properties.

2 Experimental

Stoichiometric submicron $NaNbO_3$ powders were prepared through microemulsion mediated synthesis [7] followed by an annealing treatment at 800 °C for 12 h [14]. The prepared powder was analyzed with respect to crystallinity, phase purity, composition and crystallite size based on the results from XRPD using a Philips X'Pert diffractometer ($Cu-K_\alpha$ radiation), inductively coupled plasma with optical emission spectroscopy and scanning electron microscopy (SEM). The XRPD patterns were refined by the Rietveld method (Fullprof software package [16]).

Raman spectra were recorded at various temperatures using a Jobin–Yvon T64000 Raman spectrometer equipped with a Spectrum-One CCD detection system and a microscope focusing unit. Powder samples were mounted on a quartz crucible, which was placed on a silver heating block of a THMS600 sample stage (Linkam Scientific Co.). The temperature stability of this system was better than 0.1 °C. Samples were excited using 514.5 nm radiation from a BeamLok 2060 argon ion laser (Spectra-Physics Co.) with a power below 10 mW at the sample. The spectra were obtained in backscattering geometry with an entrance slit of 100 μm, an optical system with a triple subtractive configuration and a grating with 1,800 grooves mm^{-1}.

Raman scatterings at pressure up to 15.9 GPa were collected using a diamond anvil cell. The samples were mounted together with ruby tips and a pressure medium consisting of a methanol–ethanol mixture with a volume ratio of 4:1 between the two diamonds (culet-diameter: 0.8 mm) mediated by a gasket (thickness: 0.5 mm, hole diameter: 0.4 mm). They were excited using a 532.0 nm radiation from a LD pumped Nd:YVO_4 laser (Showa optronics Co.). Raman scatterings were recorded using a NRS-1000DT Raman spectrometer (JASCO Co.) equipped with an Andor CCD detector under backscattering geometry. The wavelength shift of the fluorescence line emitted from the ruby tips (R_1 line) was monitored in order to calibrate the pressure. The obtained Raman spectra were fitted with Lorentzian functions using the Grams/AI software (Thermo Galactic Co.).

For the sample preparation for PFM-study, first micron and submicron powders were dispersed and fixed in epoxy resin. The polished powder-epoxy composites with powder exposures on the surfaces were used for the PFM measurements. In-plane displacements with increasing electric field were measured by a modified JEOL 4210 atomic force

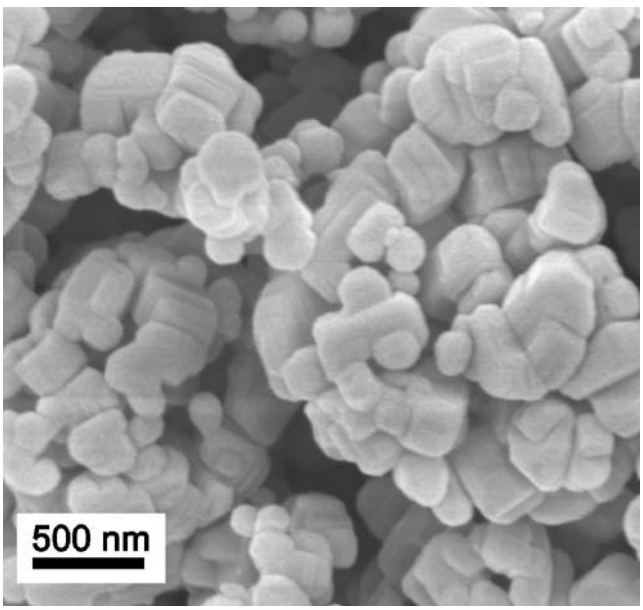

Fig. 1 SEM image obtained for the submicron $NaNbO_3$ powder

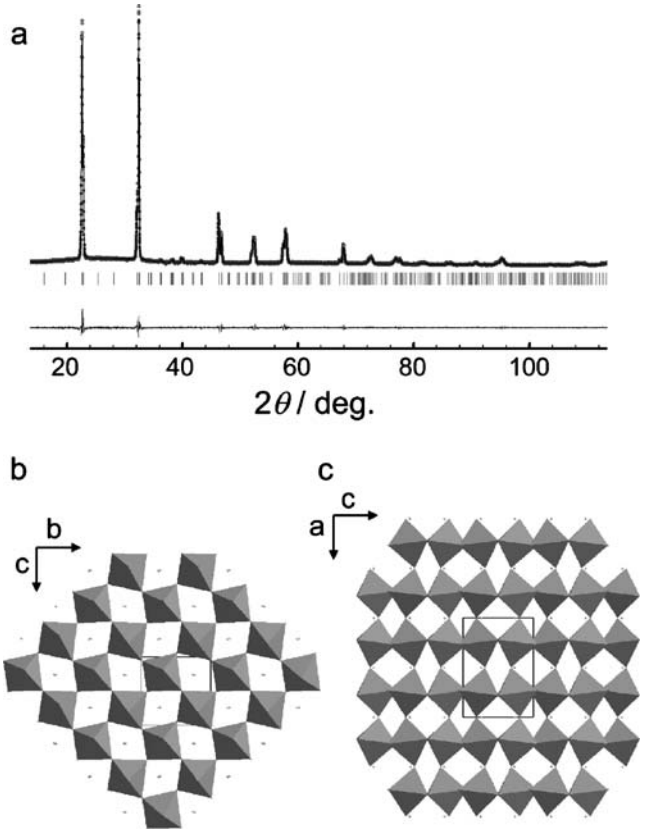

Fig. 2 **a** Rietveld refinement pattern, where *dots*, *solid line*, *tick marks* and the *bottom line* represent the measured diffraction intensity, the calculated pattern, the reflection positions and the difference between the measured and simulated spectra, respectively. Graphical views of the **b** b–c and **c** a–c planes for submicron $NaNbO_3$

microscope. A voltage of 3 VAC at 7 kHz was applied to a PtIr coated cantilever (ContPt, Nanosensors Co., resonance frequency: 13 kHz). Furthermore, the magnitude of the piezoresponse was also measured as a function of the applied generator voltage.

3 Results and discussion

Figure 1 shows a SEM image obtained for the submicron $NaNbO_3$ powder. The average particle diameter was evaluated using the line intercept method from the SEM image and its value was 0.3±0.1 μm. Figure 2a shows the experimental XRPD pattern modelled by Rietveld refinement and the difference with the registered one. The refined lattice parameters are a=0.776778(5), b=0.551759(2) and c=0.556829(2) nm for this powder. These values are in good agreement with the results from the previous structural characterization (detailed atomic coordinates are given in [14]). Therefore, the preparation of such a material is perfectly reproducible. According to the representations shown in Fig. 2b and c, the two main features of such noncentrosymmetric structure (orthorhombic $Pmc2_1$) are a significant rotation of octahedra around the a-axis and their tilt along the stacking axis.

The Raman active normal modes of the space group $Pmc2_1$ are represented by $16A_1+13A_2+12B_1+16B_2$ [14]. Therefore the submicron powders show complicated Raman scattering profiles. Figure 3 shows the evolution of the Raman spectra recorded for the submicron $NaNbO_3$ powder on sequential heating and after cooling down to −150°C. According to the assignments for bulk $NaNbO_3$ [17], the bands below 80 cm^{-1} are assigned to Na^+ translational modes against the NbO_6-octahedra. The librational and internal modes of NbO_6-octahedra appear in the regions from 80 to 160 cm^{-1} and above 160 up to 900 cm^{-1}, respectively. The number of bands decreases and the individual bands broaden with increasing temperature. Temperature-induced spectral transitions are reversible on heating and cooling. Figure 4 shows the wavenumber shift of the NbO_6 librational mode at around 118 cm^{-1}. Although most of the bands shift towards lower frequencies with increasing temperature, this mode shows a gradual shift towards a higher frequency. A drastic

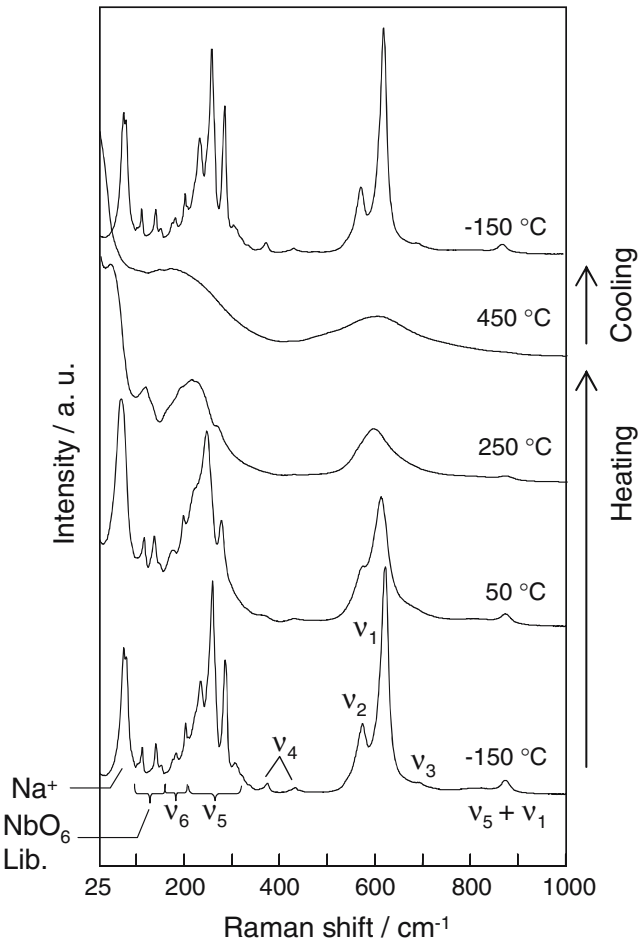

Fig. 3 Raman spectra recorded for the submicron $NaNbO_3$ powder at various temperatures upon heating and after cooling down to −150 °C. Band assignments reported for bulk material [17] are indicated below the spectra

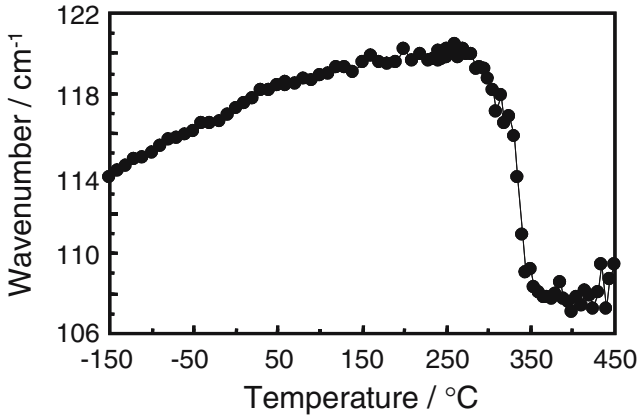

Fig. 4 Wavenumber shift of the NbO_6-librational mode on heating

softening of this mode starts at 280 °C and continues up to 360 °C. Above 360 °C the slope of temperature characteristic becomes more gradual.

Above 300 °C the Raman scattering profiles become simpler (Fig. 3). This indicates that the crystal structure transforms into a higher symmetry at high temperature. Figure 5 shows the comparison between the spectra obtained for the micron (upper) and submicron (lower) powders at 360 and 440 °C, respectively. It is known that bulk $NaNbO_3$ shows a phase transition from the antiferroelectric orthorhombic P phase to an antiferroelectric orthorhombic R phase at 373 °C [10, 18]. Exemplarily the spectra obtained for micron-sized powders recorded at 360 and 440 °C respectively are compared in Fig. 5 to those for submicron powders at the same temperatures. These temperatures have been selected representatively to show the characteristics of both powders above and below the transition point of 373 °C for the phase transformation from P to R phase of bulk $NaNbO_3$. The spectra obtained for our micron-sized powder (Fig. 5b and d) agree well with the high temperature profiles reported for bulk $NaNbO_3$ [10]. The spectrum recorded for the submicron powder at 440 °C (Fig. 5c) also shows excellent agreement with the scattering profiles obtained for the micron-sized powder. On the other hand, the spectrum obtained at 360 °C (Fig. 5a) shows a different profile compared to that measured for the coarser sample at the same temperature (Fig. 5b) but it has already the same contour as that obtained at 440 °C (Fig. 5c). Since Raman spectroscopy is very sensitive to changes of the space group, these spectral features indicate that after softening of the NbO_6 librational mode (above 360 °C, Fig. 4) the phase becomes bulk-like. Antiferroelectric (AF) to ferroelectric (FE) transition characterized by the softening of the NbO_6 librational mode through an AF–FE coexisting phase has been reported for the bulk $NaNbO_3$ sample at −88 °C [18]. In the case of the submicron $NaNbO_3$, a significant transition from a noncentrosymmetric phase toward the antiferroelectric bulk-like phase may occur through the region of coexisting phases (280–360 °C). Finally we conclude that the described phase transition behaviour is completely reversible on temperature change as long as temperature rising does not result in a coarsening of the particles.

Figure 6 shows representative Raman spectra recorded at various increasing pressures up to 15.9 GPa at room temperature. The spectra obtained after the pressure has been released and obtained for the micron-sized powder at 15.8 GPa are also indicated in Fig. 6. At an ultra high pressure of ca. 16 GPa, the spectrum profile becomes similar to that for the micron-sized powder, which has a bulk type crystallographic structure (orthorhombic *Pbcm*) at ambient pressure. Figure 7 shows representatively the wavenumber shifts for the split ν_5 and ν_4 bands of the NbO_6 internal modes (marked in Fig. 6 by a closed circle and triangle, respectively) with increasing hydrostatic pressure. Other degenerated and split bands have been omitted for the sake of clarity. The first convergence of the ν_5 bands occurs at around 2 GPa (Fig. 7a), which is followed by linear wavenumber shifts with increasing pressure up to around 6 GPa. Spectral divergence and convergence are found in the pressure region from 6 to 7 GPa. Finally some specific bands disappear and the slopes of pressure characteristics for the remaining bands change at around 10 GPa. On the other hand, the slope for the ν_4 mode changes at around 7 GPa and another change of the slope can be found at around 10 GPa (Fig. 7b). The tendency that significant structural transitions occur at around 6.5 and 10 GPa has also been reported for bulk

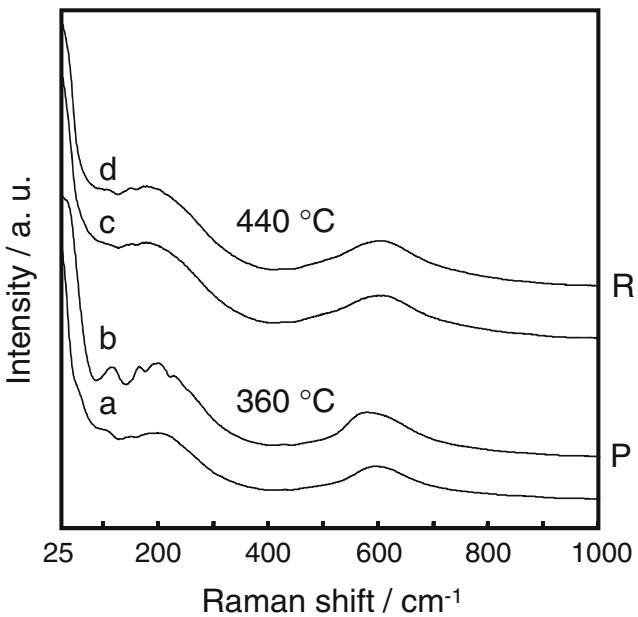

Fig. 5 Raman spectra recorded for submicron (**a**, **c**) and micron (**b**, **d**) $NaNbO_3$-powders at 360 and 440 °C. *P* and *R* indicate the orthorhombic P- and R-phases, respectively, which are assigned for bulk $NaNbO_3$ [10]

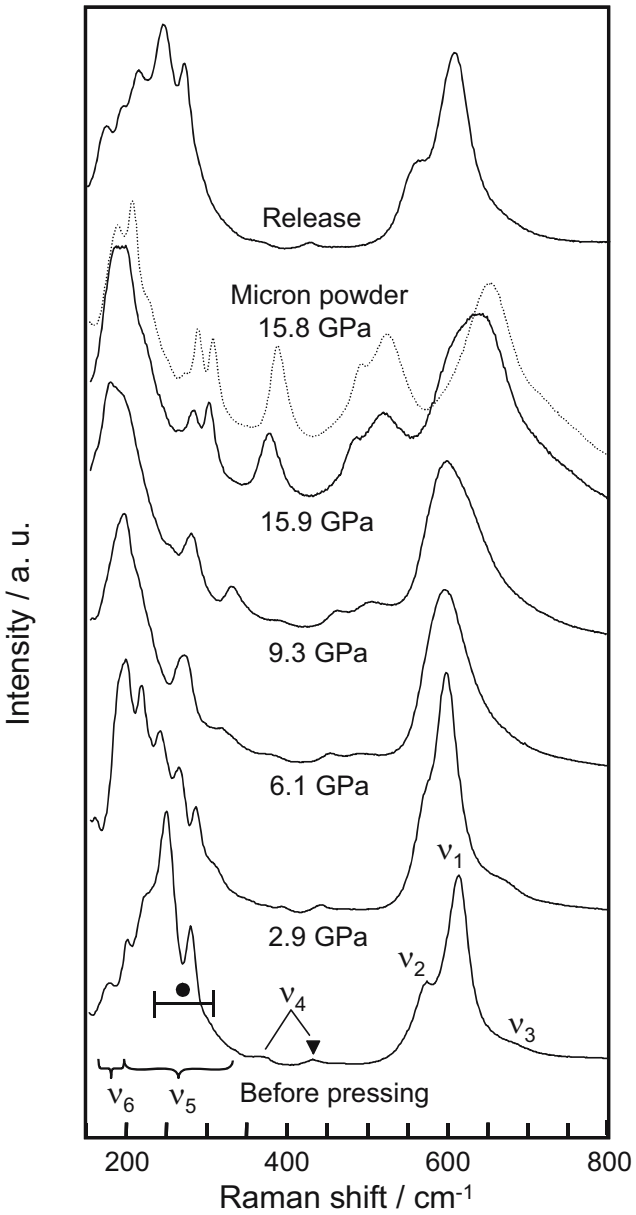

Fig. 6 Evolution of the Raman spectra upon pressing and after pressure release recorded for submicron $NaNbO_3$. The spectrum obtained for the micron $NaNbO_3$ at 15.8 GPa (*dotted curve*) is stacked above the spectrum at 15.9 GPa

$NaNbO_3$ by Shen et al. [17]. The bulk phase transforms from the room temperature orthorhombic phase (P) to a high-pressure phase I (HP I) at 7 GPa and from HP I to another high-pressure phase at 12 GPa. The similarity of the spectra obtained for the submicron $NaNbO_3$ powder at pressures above 7 GPa to those reported for bulk material suggests that pressure characteristics of the submicron powder get close to those for bulk material under high pressure. On the contrary, major differences of the pressure characteristics between the submicron powder and bulk material lie in the pressure range from 1 to 7 GPa. The main structural feature at ambient pressure is a significant rotation of octahedra around the *a*-axis (Fig. 2b). The $Pmc2_1$ structure is therefore related to the bulk-like structure through a rotational reorientation of the NbO_6-octahedra.

In the case of temperature tuning Raman spectroscopy, the reversibility is prefect: no difference can be detected between the original spectrum measured at −150 °C and that obtained after heating to high temperatures and subsequent cooling (Fig. 3). For pressure tuning Raman spectroscopy, the situation is slightly different: qualitatively both the original low-pressure spectra and those measured after pressure release correspond. Small deviations in the band positions and broadness remain when very large pressures are applied. In the case of pressing up to 15.9 GPa, the octahedral structure itself is believed to be significantly distorted from the equilateral structure. For example, considering the ν_6, ν_4, ν_3 modes, no Raman activity is predicted for the equilateral structure of the NbO_6-octahedra. If the pressure is increased up to 15.9 GPa, atomic displacements are induced for a close packed ionic structure in which Na^+ ions are believed to be already in direct contact [17] and consequently the internal modes still show intense scattering peaks ranging from 150 to 800 cm^{-1}, with intensities of comparable level. Slight displacements of atoms seem to remain after the pressing–depressing sequence and this is reflected by slight spectral

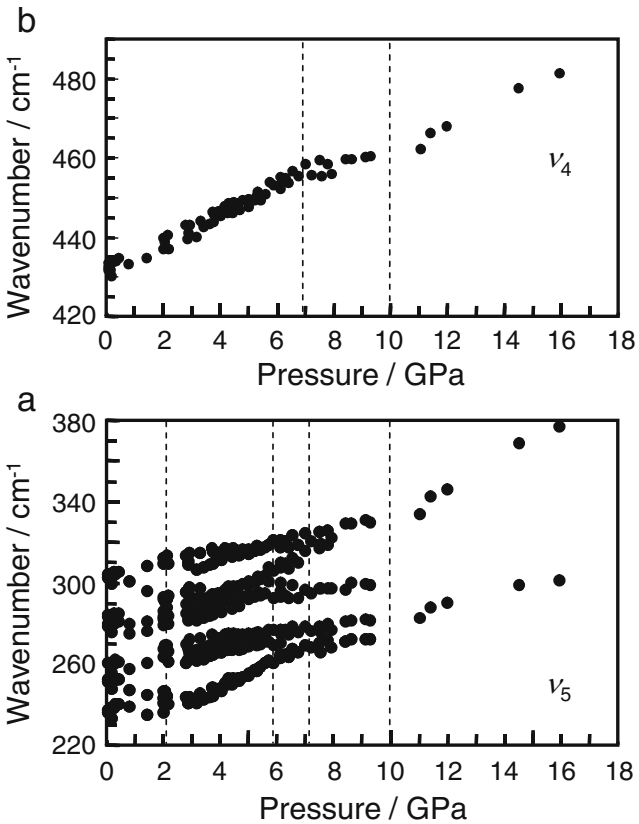

Fig. 7 Wavenumber shifts of the internal vibrational modes ν_5 and ν_4 on pressing

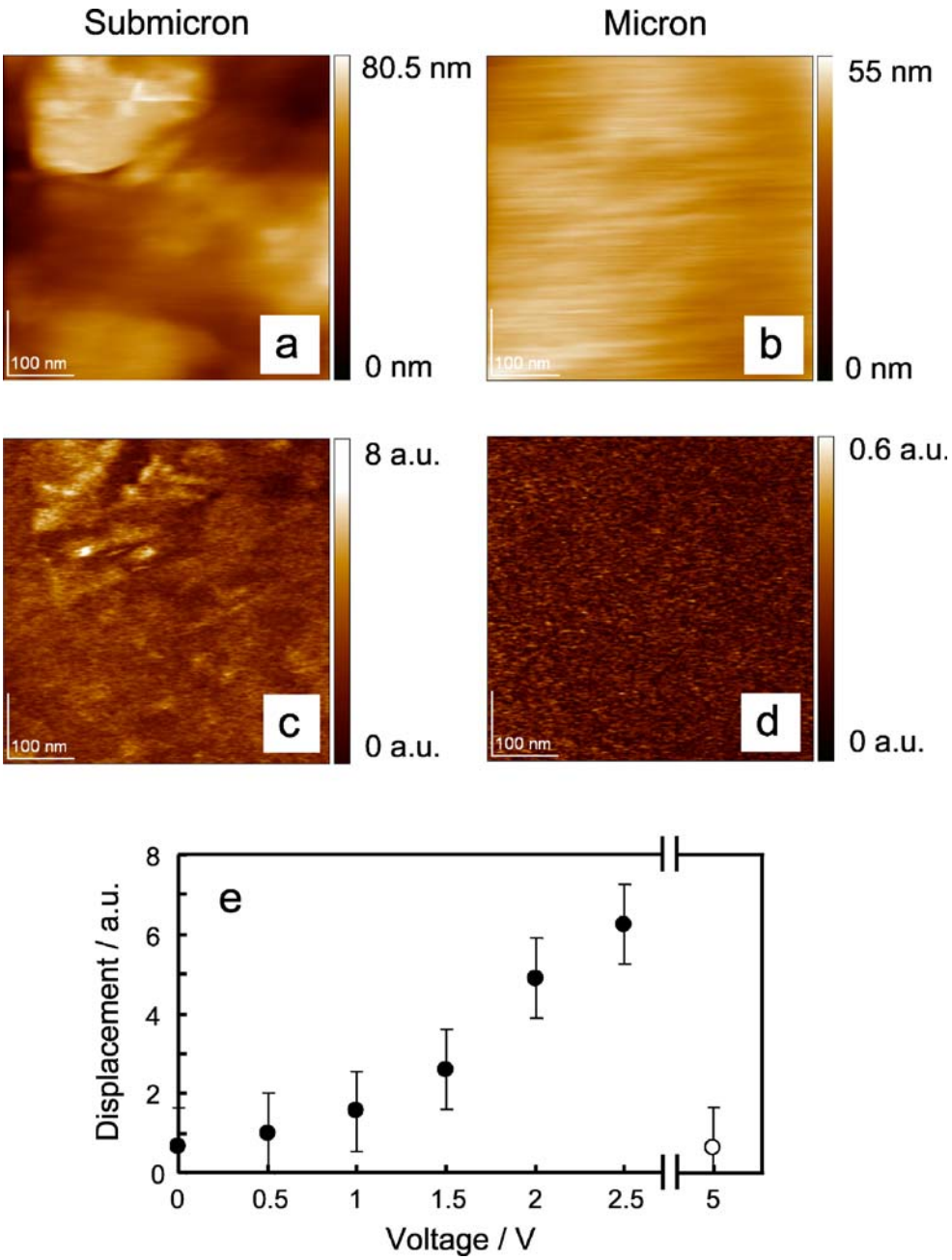

Fig. 8 Result of the AFM and in-plane PFM measurements: **a**, **b** topographical images (500 nm×500 nm), **c**, **d** mapping of and **e** voltage dependence of in-plane piezoresponse for submicron (*filled circle*) and coarse (*open circle*) $NaNbO_3$ crystals, respectively. The *error bars* indicate the maximum mechanical uncertainty with respect to the measured piezoresponse signal

changes before and after pressing. This kind of small irreversibility has also been reported for the bulk material [17]. Quite recently, we could reveal that the pressure characteristic up to ca. 1 GPa is completely reversible but a considerable irreversibility is induced by pressing over 2 GPa. Study on reversibility of transitions indicates that the orthorhombic $Pmc2_1$ polymorph is apparently stable at room temperature and ambient pressure. However, after preparation of powder samples atomic positions may deviate from a potential minimum possibly due to local stresses at each stage of crystal growth. Therefore mechanical reorientation of atomic positions may contribute to irreversible structural change. A more detailed study on this phenomenon will be reported elsewhere. To clarify the transition mechanisms, a detailed analysis focusing on the low pressure region and a thorough comparison of the phonon characteristics of the three polymorphs assigned for three different particle size regions (nano-, submicro- and microcrystalline) are necessary.

Piezoelectric materials do not present an inversion centre in the unit cells of their crystal structure. Therefore, an enhancement of converse piezoelectricity is expected for the noncentrosymmetric phase of the present study in comparison with the centrosymmetric bulk phase. A direct indication was given by a PFM-study. Powders used for this experiment were synthesized as a new batch. Two types

of powders with different particle scales were prepared through annealing treatments at 800 and 1,000 °C for 1 and 12 h, respectively. Figure 8 shows the results of a study using piezoresponse force microscopy in order to characterize the piezoactivity of both submicron and coarse reference $NaNbO_3$ crystals. Figure 8a and b show the topography of these samples monitored using the constant force mode of the microscope. In the case of the submicron sample (Fig. 8a) several grains of approximately 200–300 nm in diameter can be recognized. For example in the top left corner of Fig. 8a very clearly an almost spherical particle of ca. 200 nm can be seen. On the other hand, Fig. 8b shows a crystal which has dimensions exceeding the scanned area of this picture. The corresponding mappings of the in-plane piezoresponse signal (piezoelectric displacement parallel to the sample surface) in arbitrary units are shown in Fig. 8c and d. For the coarse reference sample (Fig. 8d) only a very small and noisy signal with maximum amplitude of 0.6 a.u. is recorded. Only very locally this low intensity response can be detected. No correlation between the response and the topography can be found. On the other hand much larger piezoelectric displacements are measured for the submicron crystals (Fig. 8c). The regions of maximum piezoactivity (e.g. white area in the top left corner of Fig. 8c) correspond to the locations of grains identified in the topography image and show a maximum signal up to 8 a.u., which is more than 10 times the value observed for the coarse reference. For a more thorough comparison of both cases, the in-plane piezoelectric displacement was measured in dependence of the excitation voltage several times using the same tip in order to reduce the influence of the tip form on the applied electric field [19]. The results are plotted in Fig. 8e. One intention of Fig. 8e is to provide evidence of a linear dependence of the strain response on the applied AC voltage as expected for piezoresponse. Even though the units are arbitrary due to the experimental setup they can be quantitatively compared as they stem from the very same cantilever (thus identical optical amplification etc.). In the case of the submicron sample (•) an almost linear correlation can be found up to 2.5 V. Due to experimental limitations (drift of the PFM-tip) only 6 values can be recorded for each of the two measuring sequences. The lack of data for voltages above 2.5 V for this sample is believed to be related only to the instability of the tip with progressing time and not to the actual value of the voltage. For the coarse reference (○) the in-plane piezoelectric response was measured several times on four different spots. In this case only signals with amplitudes ranging from 0.08 up to 0.4 a.u. can be recorded up to 5 V maximum voltage. Up to this maximum the signal is only comparable to the noise value (0.65 a.u.) of the submicron sample. The single data point (○) corresponds to the maximum piezoreponse signal of the coarse structure at 5 V and reflects (1) the low signal level that also becomes evident in the low contrast of Fig. 8d and (2) that the piezoresponse for lower voltages is within the noise level. In that sense Fig. 8 provides two sequences of measurements with a ratio of the piezoelectric response in plane of at least one order of magnitude in favour of the fine structure. A DC bias voltage would not provide a discrimination of both activities as it would be averaged out in the Lock-In driven AC detection mode.

4 Conclusions

Phase transitions induced by temperature and pressure were found for $NaNbO_3$ submicron powder at 280–360 °C and at around 2, 6.5, 10 GPa. In the case of the temperature characteristics, the transition is perfectly reversible and the high-temperature phase at 440°C corresponds to the bulk high-temperature phase. On the other hand, high-pressure phases above 7 GPa indicate bulk-like scattering contours and the transitions are almost reversible. Noncentrosymmetric phases exist below 280 °C at ambient pressure or below at least 1 GPa at room temperature. The submicron powder showed an enhanced piezoelectric activity which is significantly larger in comparison to the micron powder. Noncentrosymmetry of pure $NaNbO_3$ results in an improvement of piezoresponse for this generally antiferroelectric material.

Acknowledgements One of the authors (Y.S.) sincerely acknowledges the Alexander von Humboldt Foundation (Bonn, Germany) for granting financial support through a Research Fellowship. We gratefully thank Dr. Jürgen Dornseiffer (Institut für Chemie und Dynamik der Geosphäre II, Forschungszentrum Jülich GmbH, Jülich, Germany) and Dr. Franz-Hubert Haegel (NanDOx, Germany) for powder synthesis and Mr. Jochen Friedrich (Institut für Festkörperforschung, Forschungszentrum Jülich GmbH, Jülich, Germany) for SEM studies.

References

1. E. Cross, Nature **432**, 24 (2004)
2. Y. Saito, H. Takao, T. Tani, T. Nonoyama, K. Takatori, T. Homma, T. Nagaya, M. Nakamura, Nature **432**, 84 (2004)
3. Y. Shiratori, A. Magrez, C. Pithan, Chem. Phys. Lett. **391**, 288 (2004)
4. E. Ringgaard, T. Wurlitzer, J. Eur. Ceram. Soc. **25**, 2701 (2005)
5. D. Jenko, A. Benèan, B. Maliè, J. Holc, M. Kosec, Microsc. Microanal. **11**, 572 (2005)
6. T. Hungría, L. Pardo, A. Moure, A. Castro, J. Alloys Comp. **395**, 166 (2005)
7. C. Pithan, Y. Shiratori, J. Dornseiffer, F.-H. Haegel, A. Magrez, R. Waser, J. Cryst. Growth **280**, 191 (2005)
8. C. Pithan, T. Schneller, Y. Shiratori, S.B. Majumder, F.-H. Haegel, J. Dornseiffer, R. Waser, Int. J. Mat. Res. (formerly Z. Metallkd) **97**, 499 (2006)
9. B. Jaffe, W. R. Cook, H. Jaffe, *Piezoelectric Ceramics.* (Academic, London, 1971), p. 193

10. X.B. Wang, Z.X. Shen, Z.P. Hu, L. Qin, S.H. Tang, M.H. Kuok, J. Mol. Struct. **385**, 1 (1996)
11. E. Bouziane, M.D. Fontana, M. Ayadi, J. Phys.: Condens. Matter **15**, 1387 (2003)
12. W.L. Zhong, P.L. Zhang, H.S. Zhao, Z.H. Yang, Y.Y. Song, H.C. Chen, Phys. Rev. B **46**, 10583 (1992)
13. Y.D. Juang, M.L. Hu, W.S. Tse, J. Appl. Phys. **76**, 3746 (1994)
14. Y. Shiratori, A. Magrez, J. Dornseiffer, F.-H. Haegel, C. Pithan, R. Waser, J. Phys. Chem. B **109**, 20122 (2005)
15. H. Xu, Y. Su, M.L. Balmer, A. Navrotsky, Chem. Mater. **15**, 1872 (2003)
16. T. Roisnel, J. Rodriguez-Carjaval, Physica B. **192**, 55, (1993)
17. Z.X. Shen, X B. Wang, S.H. Tang, M.H. Kuok, R. Malekfar, J. Raman Spectrosc. **31**, 439 (2000)
18. Z.X. Shen, X.B. Wang, M.H. Kuok, S.H. Tang, J. Raman Spectrosc. **29**, 379 (1998)
19. F. Peter, A. Rüdiger, R. Dittmann, R. Waser, K. Szot, B. Reichenberg, K. Prume, Appl. Phys. Lett. **87**, 082901 (2005)